Supporting information

$Ti_3C_2T_x$ and copper sulfide composite nanofluid with hierarchical structure for sustainable and efficient solar light-thermal conversion

Fangfang Su, Zhongjie He, Jinliang Xie, Jing Zhang, Weirui Zhang, Yangyang Xin, Aibo Zhang, Dongdong Yao*, Yaping Zheng*

School of Chemistry and Chemical Engineering, Northwestern Polytechnical University Xi'an, Shaanxi 710072, P. R. China, Telephone and fax numbers: +86-029-88431688

* Corresponding authors. E-mail: yaodd@nwpu.edu.cn (D. Yao), zhengyp@nwpu.edu.cn (Y. Zheng)

1. Experimental part

1.1 Light-thermal conversion performance test

In this work, the nanofluid was placed in a container, and illuminated by a solar simulator MICROSOLAR300 xenon light source (Beijing Perfectlight Technology Co., Ltd., China) with different light intensity, and its temperature changes were recorded through a data collector. Turn off the light source after the temperature reaches equilibrium, cool the nanofluid to room temperature. In addition, the temperature changes of nanofluids are recorded using an infrared thermal imager Fotric 225s.

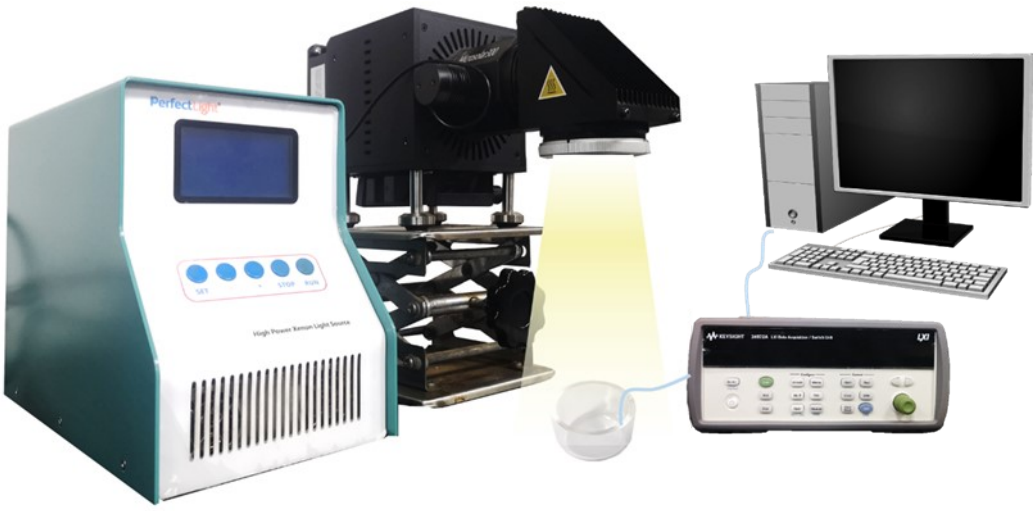

Fig. S1 Light-thermal conversion performance testing device diagram.

1.2 Water evaporation performance test

The water evaporation experiment was performed using a solar simulator MICROSOLAR300 xenon light source (Beijing Perfectlight Technology Co., Ltd., China) outputting a simulated solar intensity of 1.0-3.0 kW/m^2 with an air mass (AM) 1.5 G filter and an interfacial evaporator as schematically illustrated in Fig. S2. Float the dialysis bag on the surface of 30 mL pure water, and 1.5 g of nanofluid was placed above the dialysis bag to form an interface evaporator. Finally, place the interface evaporator on an electronic balance (SY204, Shanghai Yoke Instrument Co., Ltd) with an accuracy of ±0.1 mg to detect changes in water quality. Use CEL-NP2000 optical power meter (China Education Au light Technology Co., Ltd., China) to detect changes in light intensity. The water evaporation rate (E) and solar-to-vapor conversion efficiency (η_E) are calculated using the following equation:

$$E = \frac{\Delta m}{S \cdot t} \tag{S1}$$

$$\eta_E = \frac{E \cdot H_{L-v}}{S_m} \tag{S2}$$

$$H_{L-v} = H_s + H_e \tag{S3}$$

$$H_s = C(T_i - T_0) \tag{S4}$$

where Δm is the mass loss of water, S is the illuminated area of the evaporator, t is the illumination time, S_m is the illumination intensity. In addition, H_{L-v} is the enthalpy of liquid-vapor phase transition. H_{L-v} was calculated by eq. S3 and S4, where H_s is the sensible heat per unit mass of water, C is the specific heat capacity of water (4.2 J/(g·k)), T_i is the final temperature of the sample surface, and T_0 is the initial temperature of water. H_e is the phase transition enthalpy of water at T_i.

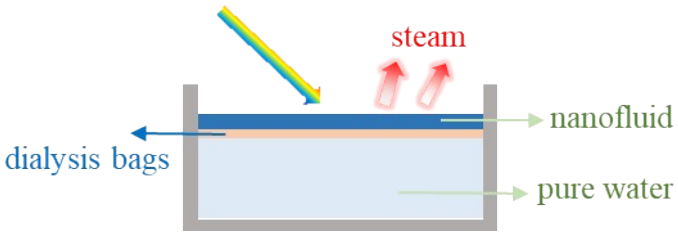

Fig. S2 Schematic diagram of water evaporation performance testing device.

1.3 Preparation of [EBIM]NTf_2

[EBIM]NTf_2 was prepared according to the methods reported in previous literature. Firstly, 150 mL of ethylacetate was measured and place it in a three necked flask as the reaction solvent. Subsequently, 0.01 mol 1-butylimidazole and 0.012 mol bromoethane were added, and reacted 24 h at 55 ℃ after mixed evenly. After the reaction was completed, the liquid undergoes layering phenomenon after being allowed to stand for a period of time. [EBIM]Br was obtained through wash the lower sediment repeatedly with ethylacetate, and dried it in a 70 ℃ oven. Afterwards, [EBIM]NTf_2 was prepared through anion exchange. Specifically, 0.01 mol [EBIM]Br was dispersed in H_2O, and then added to 50 mL of H_2O containing 0.011 mol of $LiNTf_2$. The reaction was carried out under magnetic stirring at 65 ℃ for 24 h, and the resulting lower layer precipitate can be prepared by washing and drying with water.

2. Characterization of MXene

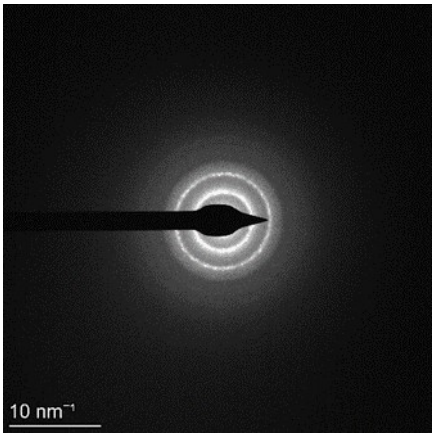

Fig. S3 Selected area electron diffraction diagram of FCuS.

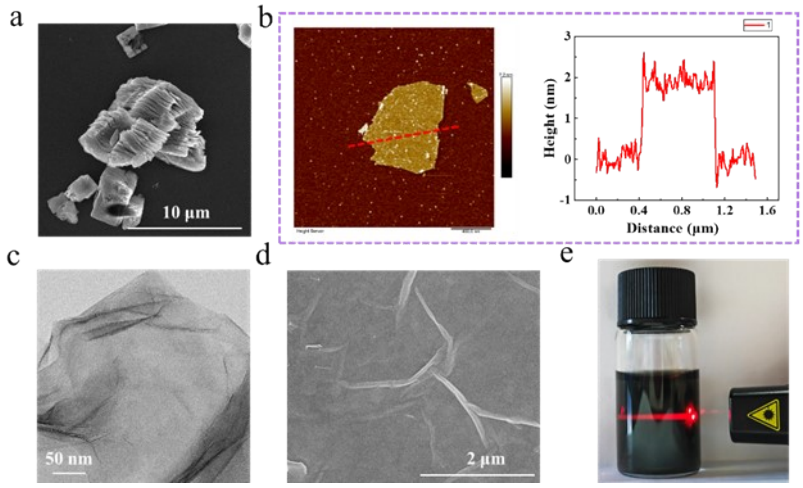

Fig. S4 (a) SEM image of accordion shaped MXene. (b) AFM image of $Ti_3C_2T_x$ nanosheet. (c, d) TEM and SEM images of $Ti_3C_2T_x$. (e) The Tyndall effect of MXene aqueous solution.

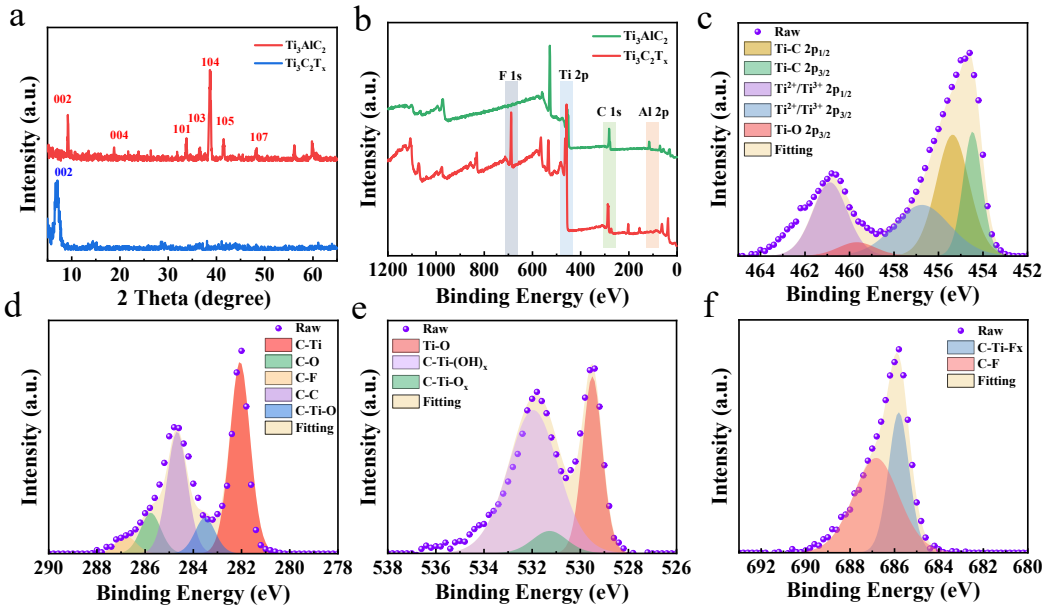

Fig. S5 (a) The XRD patterns of Ti_3AlC_2 and $Ti_3C_2T_x$. (b) The wide scan spectra of XPS of Ti_3AlC_2 and $Ti_3C_2T_x$ and elemental scan of (c) Ti, (d) C, (e) O and (f) F.

3. Characterization of [EBIM]NTf$_2$

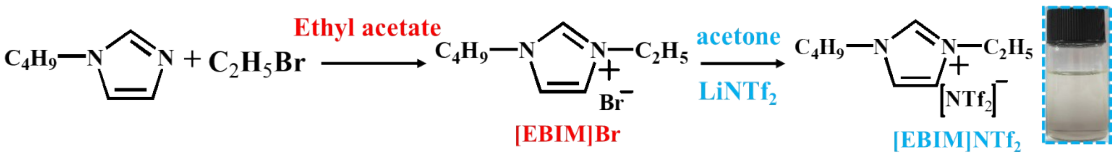

Fig. S6 Schematic diagram of [EBIM]NTf$_2$ preparation.

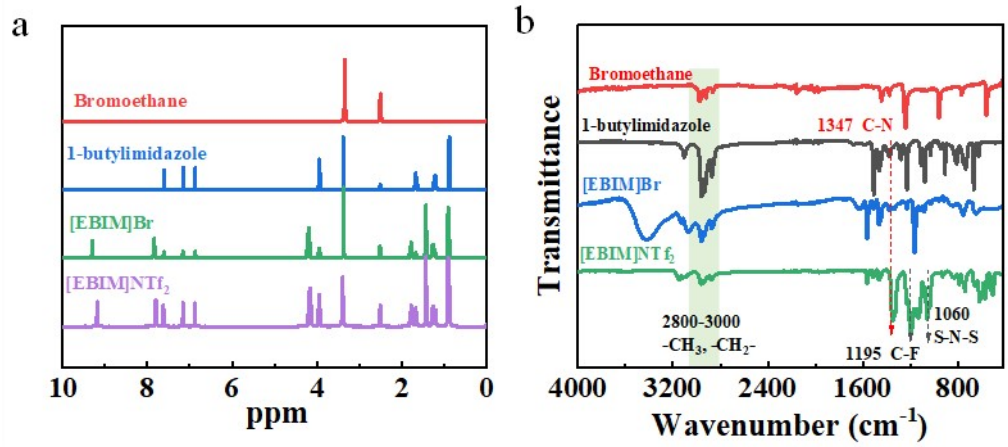

Fig. S7 (a) ^{1}H NMR spectrum and (b) FT IR spectra of bromoethane, 1-butylimidazole, [EBIM]Br and [EBIM]NTf$_2$.

4. Characterization of $Ti_3C_2T_x$/FCuS-IL and $Ti_3C_2T_x$/HCuS-IL nanofluids

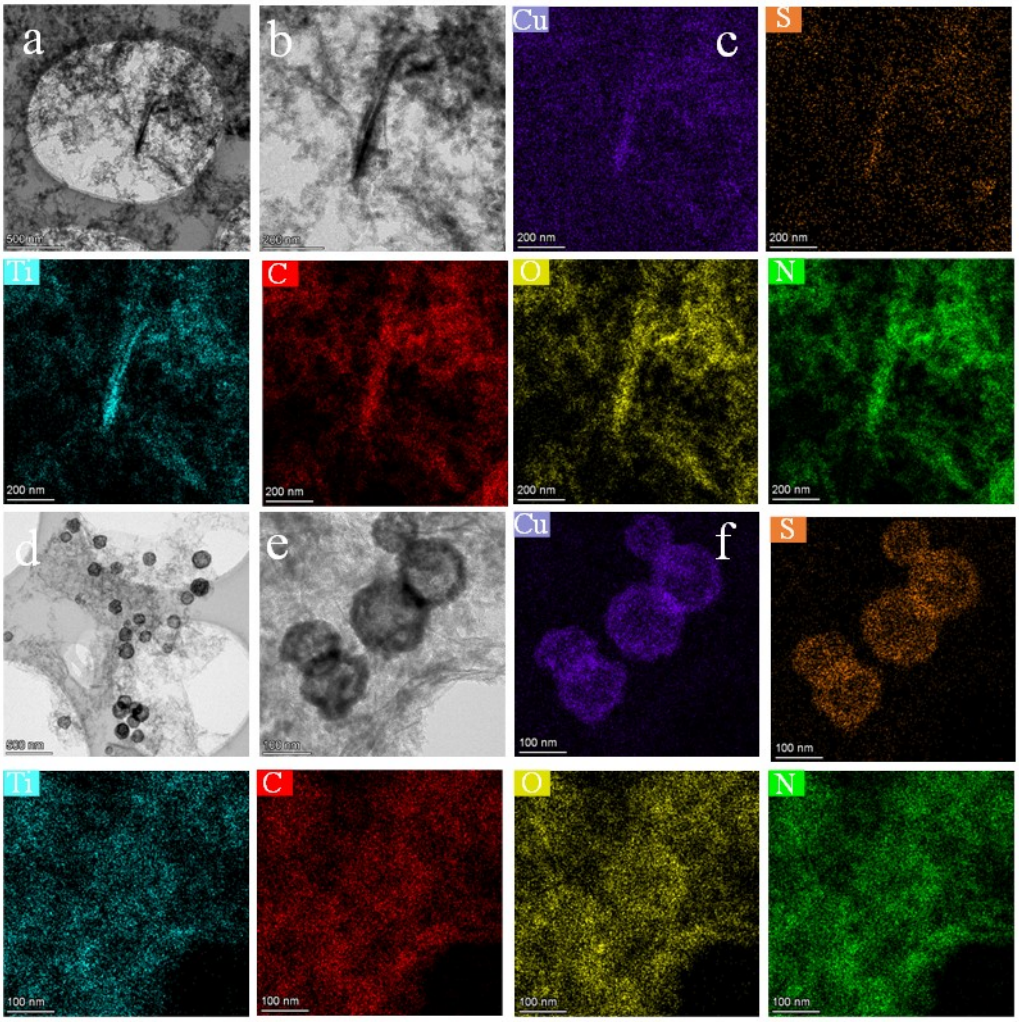

Fig. S8 (a, b) TEM images of $Ti_3C_2T_x$/FCuS-PDA. (c) The mapping analysis results of $Ti_3C_2T_x$/FCuS-PDA. (d, e) TEM images of $Ti_3C_2T_x$/HCuS-PDA. (f) The mapping

analysis results of $Ti_3C_2T_x$/HCuS-PDA.

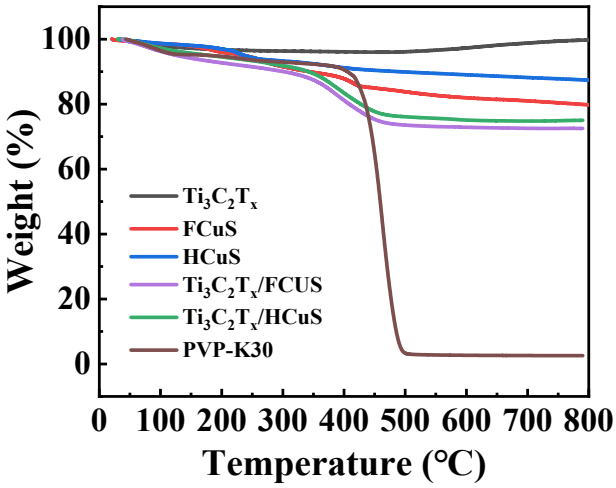

Fig. S9 The TGA curves of $Ti_3C_2T_x$, FCuS, HCuS, $Ti_3C_2T_x$/FCuS, $Ti_3C_2T_x$/HCuS and PVP-K30.

Table S1 Specific surface area of different samples

Sample	Specific surface area (m^2/g)
$Ti_3C_2T_x$	11.677
FCuS	88.95
HCuS	28.226
$Ti_3C_2T_x$/FCuS	152.707
$Ti_3C_2T_x$/HCuS	120.682
$Ti_3C_2T_x$/FCuS-PDA	238.319
$Ti_3C_2T_x$/HCuS-PDA	211.199

Fig. S10 Infrared thermal imaging of the cold platform surface.

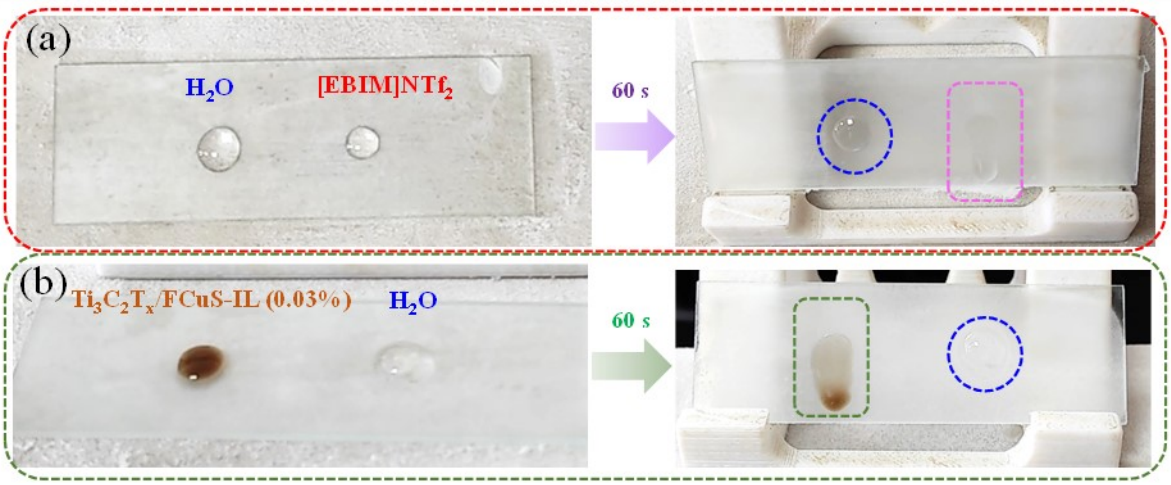

Fig. S11 Optical photos of H_2O, [EBIM]NTf_2, and $Ti_3C_2T_x$/FCuS-IL (0.12%) nanofluid placed on a cold bench for 60 s.

Fig. S12 Optical photos of [EBIM]NTf_2 and $Ti_3C_2T_x$/FCuS-IL (0.12%) nanofluids dripping with a 5 mL syringe

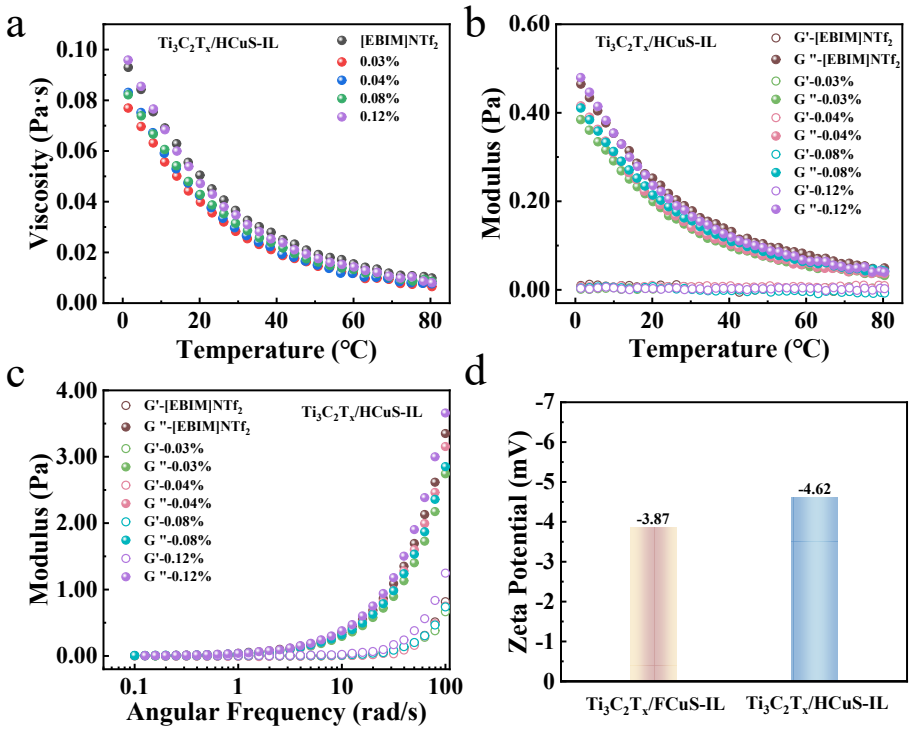

Fig. S13 (a) The viscosity-temperature curves, (b) modulus-temperature curves and (c) modulus-angular frequency curves of $Ti_3C_2T_x$/HCuS-IL. (d) The Zeta potential of $Ti_3C_2T_x$/FCuS-IL and $Ti_3C_2T_x$/HCuS-IL.

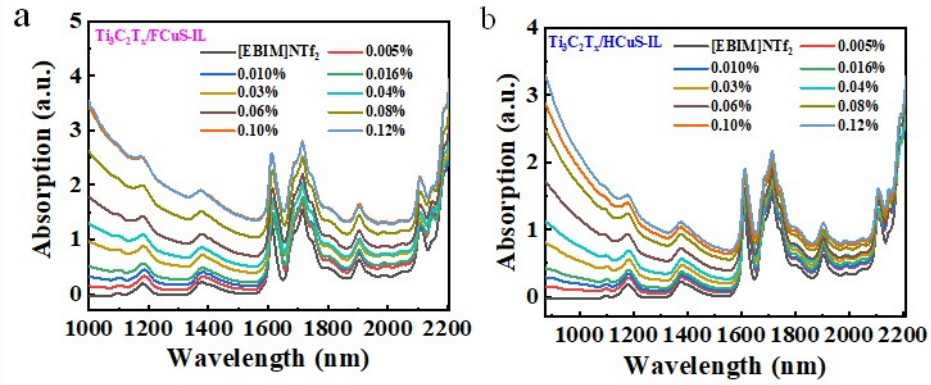

Fig. S14 Absorption of (a) $Ti_3C_2T_x$/FCuS-IL and (b) $Ti_3C_2T_x$/HCuS-IL, respectively.

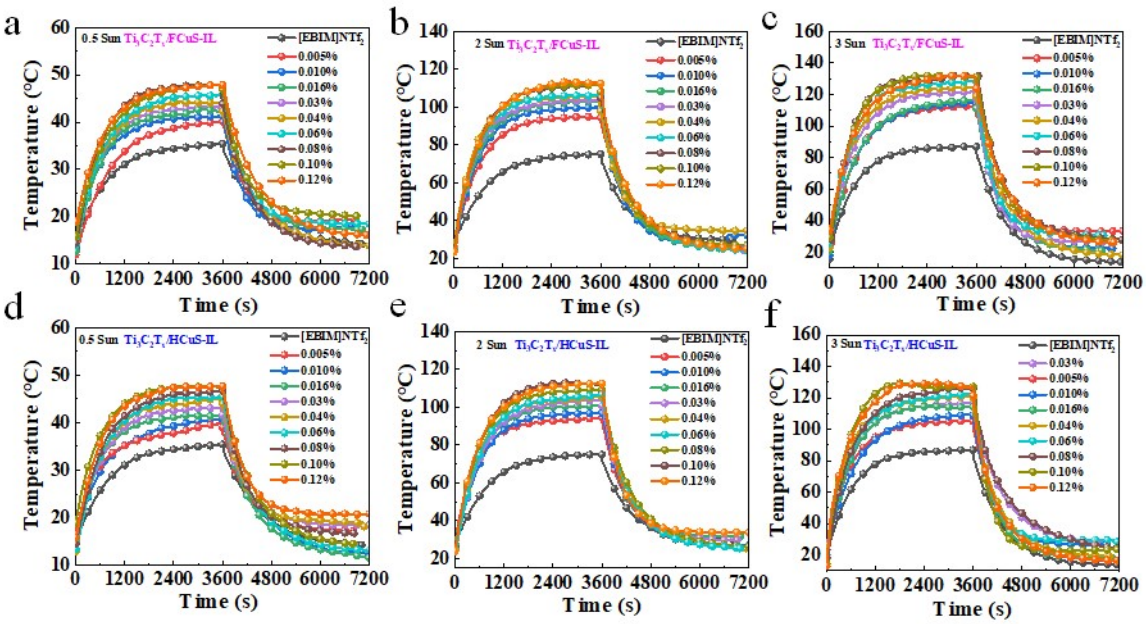

Fig. S15 Temperature dependence curves of (a-c) $Ti_3C_2T_x$/FCuS-IL and (d-f) $Ti_3C_2T_x$/FCuS-IL under different light intensities irradiation (0.5 Sun, 2 Sun, 3 Sun).

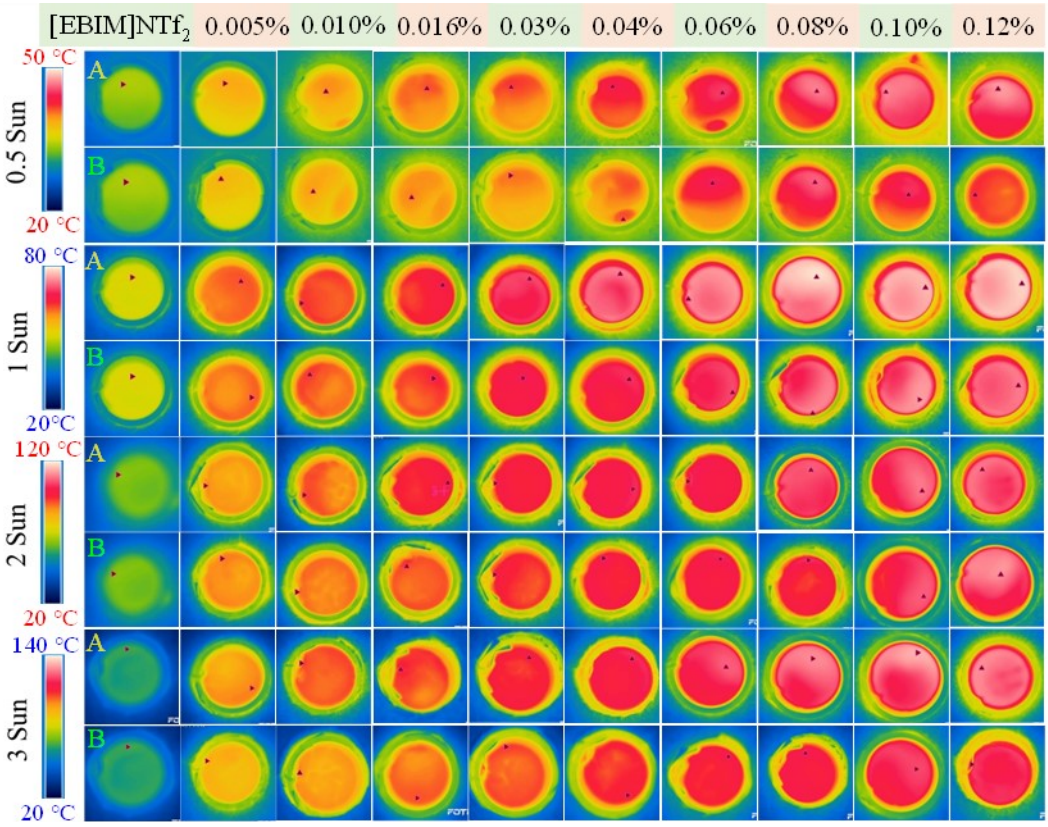

Fig. S16 Infrared thermal imaging of [EBIM]NTf_2, $Ti_3C_2T_x$/FCuS-IL and $Ti_3C_2T_x$/HCuS-IL with different mass fraction of $Ti_3C_2T_x$/FCuS and $Ti_3C_2T_x$/HCuS after irradiated at different light intensities (0.5 Sun, 1 Sun, 2 Sun and 3 Sun) for 1 h.

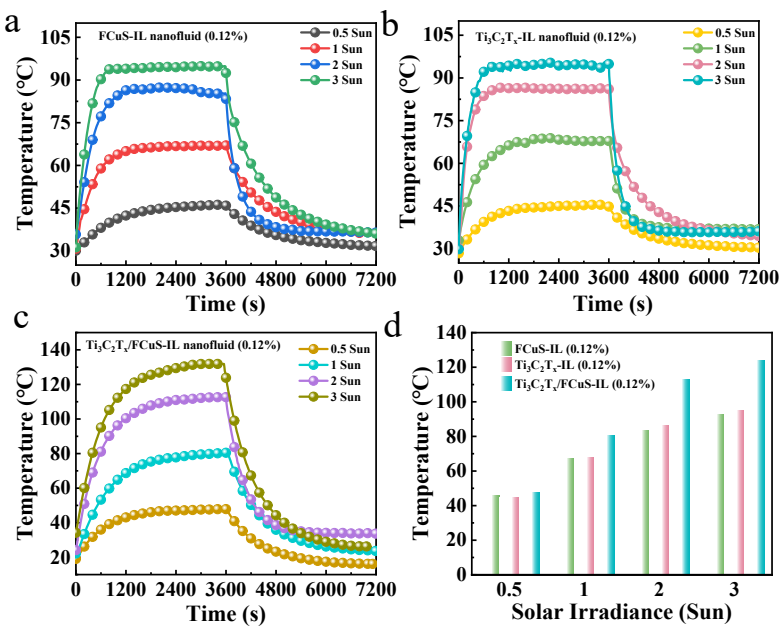

Fig. S17 Temperature dependence curves of (a) FCuS-IL, (b) $Ti_3C_2T_x$-IL and (c) $Ti_3C_2T_x$/FCuS-IL under different light intensities irradiation. (d) T_{max} of CuS-IL,

$Ti_3C_2T_x$ -IL and $Ti_3C_2T_x$/FCuS-IL after 1 h of exposure to different solar intensities.

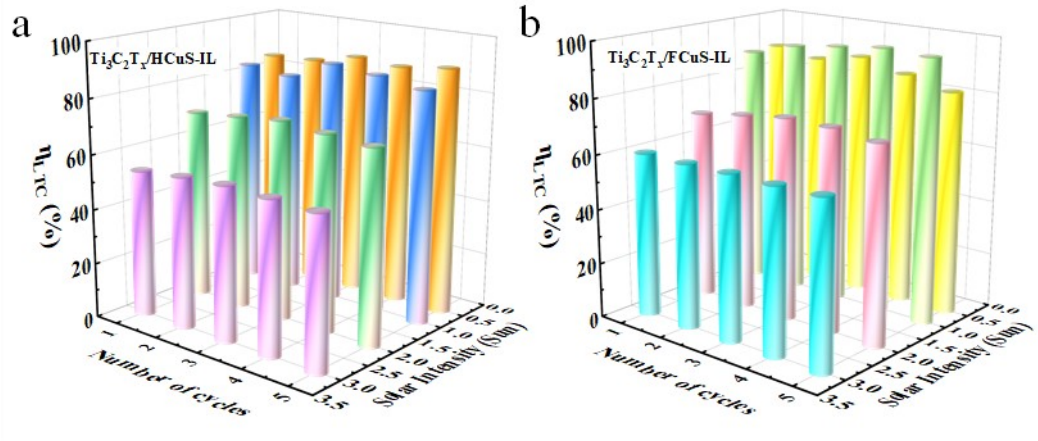

Fig. S18 The cyclic η_{LTC} of (a) $Ti_3C_2T_x$/FCuS-IL (0.12%) and (b) $Ti_3C_2T_x$/HCuS-IL (0.12%) under different solar intensity (0.5 Sun, 1 Sun, 2 Sun and 3 Sun).

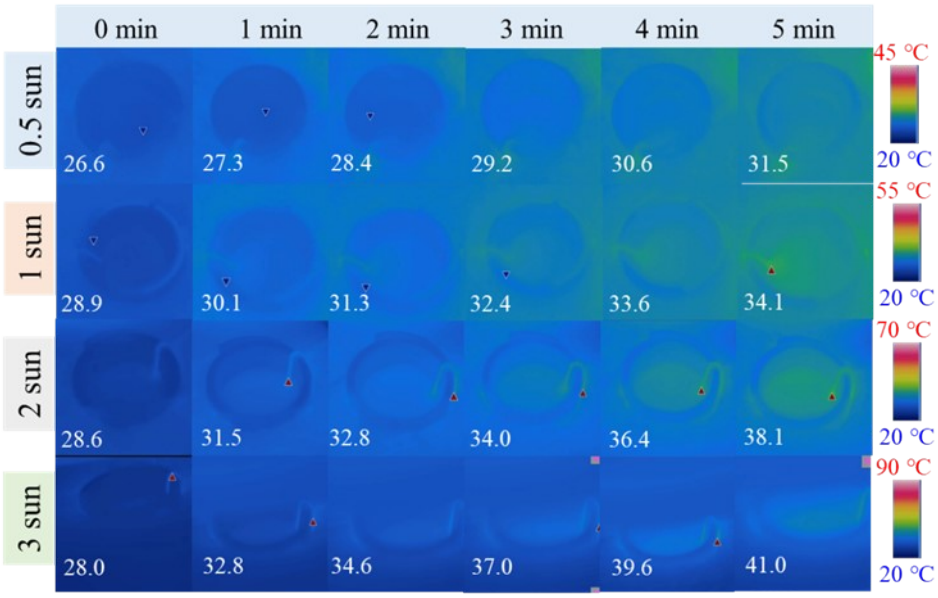

Fig. S19 Infrared thermal imaging changes of [EBIM]NTf_2 IL under different solar intensities for 5 min.

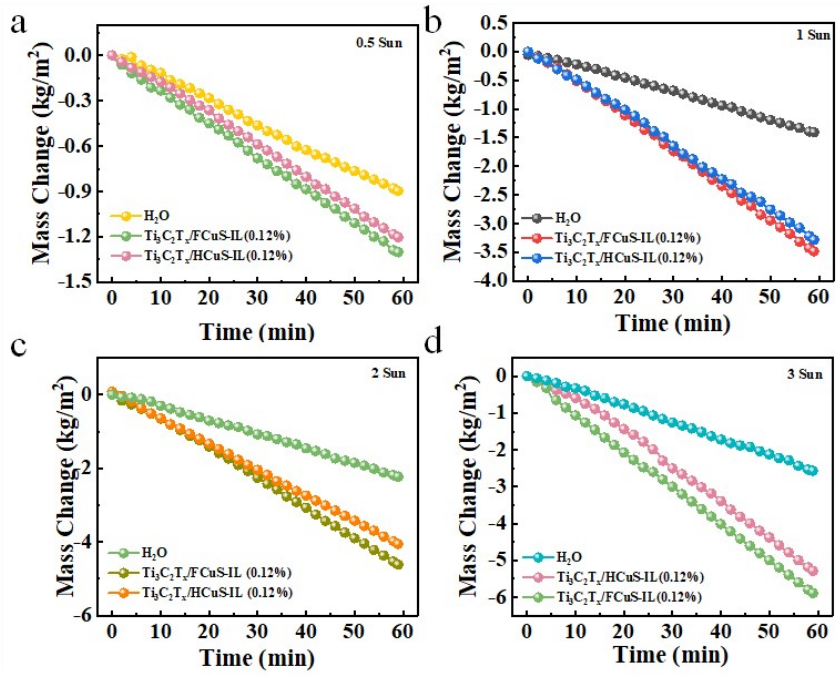

Fig. S20 Mass change of water within 60 min of exposure to different light intensities (a) 0.5 Sun, (b) 1 Sun, (c) 2 Sun and (d) 3 Sun.

Fig. S21 Separation and reused the photoabsorbers after the experiments

Table S2 Comparison of light-thermal conversion performance with previously reported literature

Materials	Test conditions	ΔT (°C)	η (%)	References
MXene nanofluid	1 Sun 0.002%	-	63.35	[1]
MXene nanofluid	1 Sun 0.02%	22	80	[2]
AuNP solutions	1 Sun	6	80	[3]

	0.2 mM			
TiO_2 nanofluid	1 Sun 2.0%	15	40	[4]
Co@NC-900 nanofluid	1 Sun 0.01%	25	45	[5]
$Ti_3C_2T_x$/PDA-IL	1 Sun 0.04%	47.9	83.93	[6]
magnetic FCNTs nanofluids	2 Sun 0.01%	11.5	-	[7]
TiN/MWCNTs hybrid nanofluids	1 Sun 0.004%	11	76.4	[8]
ZrC/TiN nanofluids	1 Sun 0.016%	22	73.7	[9]
Ag@Fe_3O_4 nanofluids	2 Sun 0.03%	23	-	[10]
MWCNT-DW/EG nanofluids	1 Sun 0.05%	38	92.0	[11]
Fe_3O_4/CNTs nanofluids	2 Sun 0.015%	14	92.1	[12]
PR nanosheets nanofluid	1 Sun 1.0%	50	-	[13]
$Ti_3C_2T_x$/FCuS-IL	1 Sun 0.08%	60.2	94	This work
$Ti_3C_2T_x$/HCuS-IL	1 Sun 0.10%	56.3	88.1	

Table S3 Comparison of water evaporation performance with previously reported literature

Materials	Evaporation	Water	Solar-to-vapor	References

	conditions	evaporation rate (kg/(m^2·h))	conversion efficiency (%)	
PDA@MXene	1 Sun	1.276	85.2	[14]
	3 Sun	4.0	90%	
carbon aerogels	1 Sun	1.29	87.51	[15]
CBS-Ti_3C_2	1 Sun	1.32	91.9	[16]
	3 Sun	3.84	88.2	
G1 MXene nanocoating	1 Sun	1.37	-	[17]
MXene/PDA@ TiO_2/Fe_3O_4@ C22-HMC	1 Sun	2.09	94.44	[18]
	3 Sun	6.36	95.85	
Janus hydrogel-1	1 Sun	1.45	-	[19]
CB-Wood	1 Sun	2.52	75	[20]
Janus PMX membrane	1 Sun	1.4	80	[21]
PPy/MXene-PDA-fabric	1 Sun	1.55	90	[22]
MXene/CIS	1 Sun	1.5	91	[23]
	2 Sun	2.5	80	
MXene/cellulose	1 Sun	1.44	91.5	[24]
Fe_3O_4/CNTs nanofluids	2 Sun	0.9	89	[12]
$Ti_3C_2T_x$/FCuS-IL (0.12%)	1 Sun	1.34	93	This work
	3 Sun	2.26	53.8	
$Ti_3C_2T_x$/HCuS-IL (0.12%)	1 Sun	1.26	87	
	3 Sun	2.03	48	

References

1. H. Wang, X. Li, B. Luo, K. Wei and G. Zeng, *Energy*, 2021, **227**, 120483.
2. X. Li, H. Chang, L. Zeng, X. Huang, Y. Li, R. Li and Z. Xi, *Energy Convers. Manag.*, 2020, **226**, 113515.
3. K. Jiang, D. A. Smith and A. Pinchuk, *J. Phys. Chem. C*, 2013, **117**, 27073-27080.
4. H. Wu, Y. Yan, J. Zhao, W. Sun, S. Zhang, W. Huang, F. Liu and C. Liu, *ACS Sustain. Chem. Eng.*, 2022, **10**, 16985-16994.
5. D. Wang, L. Wang, G. Zhu, W. Yu, J. Zeng, X. Yu, H. Xie, G. Xian and Q. Li, *ACS Appl. Energy Mater.*, 2018, **1**, 3860-3868.
6. F. Su, J. Xie, X. Li, Z. He, H. Wang, J. Zhang, Y. Xin, A. Zhang, D. Yao and Y. Zheng, *ACS Appl. Mate.r Interfaces*, 2023, **15**, 14316-14328.
7. Z. Tang, L. Yue, C. Qi and L. Liang, *Colloids Surf. A: Physicochem. Eng. Aspects*, 2023, **670**, 131623.
8. R. Yang, X. Li, F. Yin, J. Shi and D. Jing, *Int. J. Heat Mass Tran.*, 2023, **208**, 14056.
9. J. Wen, Q. Chang, J. Zhu, R. Cui, C. He, X. Yan and X. Li, *Renew. Energ.*, 2023, **206**, 676-685.
10. J. Yu, Y. Wang, C. Qi and W. Zhang, *Sol. Energy Mater. Sol. Cells*, 2023, **258**, 112434.
11. B. Sun, X. Xu, D. Yang and H. Li, *Appl. Ther. Eng.*, 2023, **230**, 120786.
12. Z. Tang, L. Chen, C. Qi and Z. Tian, *Powder Technol.*, 2022, **407**, 117691.
13. T. Shi, M. Zhang, H. Liu and X. Wang, *Sol. Energy Mater. Sol. Cells*, 2022, **248**, 112016.
14. X. Zhao, X.-J. Zha, L.-S. Tang, J.-H. Pu, K. Ke, R.-Y. Bao, Z.-y. Liu, M.-B. Yang and W. Yang, *Nano Res.*, 2019, **13**, 255-264.
15. H. Wang, A. Du, X. Ji, C. Zhang, B. Zhou, Z. Zhang and J. Shen, *ACS Appl. Mater. Interfaces*, 2019, **11**, 42057-42065.
16. Z. Wang, K. Yu, S. Gong, H. Mao, R. Huang and Z. Zhu, *ACS Appl. Mater.*

Interfaces, 2021, **13**, 16246-16258.

17. K. Li, T. H. Chang, Z. Li, H. Yang, F. Fu, T. Li, J. S. Ho and P. Y. Chen, *Adv. Energy Mater.*, 2019, **9**, 1901687.
18. Z Zheng, W Li, H Liu, X Wang, *ACS Appl. Mater. Interfaces*, 2022, **14**, 50966-50981.
19. Y. Zhang, T. Ma, F. Zhang, W. Guo, K. Yu, C. Yang and F. Qu, *J. Colloid Interface Sci.*, 2022, **607**, 1446-1456.
20. L. Fu, X. Zhou, L. Deng, M. Liao, S. Chen, H. Wang and L. Wang, *Desalination*, 2023, **550**, 116362.
21. B Zhang, Q Gu, C Wang, Q Gao, J Guo, P Wong, C Liu, A An, *ACS Appl. Mater. Interfaces*, 2021, **13**, 3762-3770..
22. J. Su, P. Zhang, R. Yang, B. Wang, H. Zhao, W. Wang and C. Wang, *Renew. Energ.*, 2022, **195**, 407-415.
23. Y. Wang, J. Nie, Z. He, Y. Zhi, X. Ma and P. Zhong, *ACS Appl. Mater. Interfaces*, 2022, **14**, 5876-5886.
24. X. J. Zha, X. Zhao, J. H. Pu, L. S. Tang, K. Ke, R. Y. Bao, L. Bai, Z. Y. Liu, M. B. Yang and W. Yang, *ACS Appl. Mater. Interfaces*, 2019, **11**, 36589-36597.